Journal of ELECTRONIC MATERIALS, Vol. 41, No. 12, 2012
DOI: 10.1007/s11664-012-2200-9

Development and Evaluation of Direct Deposition of Au/Pd(P) Bilayers over Cu Pads in Soldering Applications

C.E. HO,[1,4] T.T. KUO,[1,2] W. GIERLOTKA,[1] and F.M. MA[1,3]

1.—Department of Chemical Engineering & Materials Science, Yuan Ze University, Chungli City, Taiwan, ROC. 2.—Taiwan Uyemura Limited Company, Dayuan Township, Taoyuan County, Taiwan, ROC. 3.—School of Materials Science & Engineering, Beihang University, Beijing, China. 4.—e-mail: ceho1975@hotmail.com

The thermal reliability of Sn-3Ag-0.5Cu/Au/Pd(P)/Cu solder joints was evaluated in this study. After reflow and subsequent solid-state aging (180°C), the reaction product species at the interface included Cu_6Sn_5 [or $(Cu,Pd)_6Sn_5$] and Cu_3Sn, and their growth was strongly dependent on the Pd(P) thickness, $\delta_{Pd(P)}$. As $\delta_{Pd(P)}$ increased, the growth of Cu_6Sn_5 was significantly enhanced, while that of Cu_3Sn was suppressed. Computer coupling of phase diagrams and thermochemistry (CALPHAD) analysis showed that minor incorporation of Pd (~2 at.%) into the Cu_6Sn_5 phase decreased the Gibbs free energy of Cu_6Sn_5 from −7339 J/mol to −9191 J/mol. This effect might enhance Sn diffusion in Cu_6Sn_5 but diminish Cu diffusion in Cu_3Sn, thereby facilitating the growth of Cu_6Sn_5 but retarding that of Cu_3Sn. High-speed ball shear (HSBS) test results showed that the mechanical properties of the solder joints were slightly enhanced by an increase in $\delta_{Pd(P)}$. These findings suggest that direct deposition of Au/Pd(P) bilayers over the Cu pads can effectively modify the mechanical reliability of solder joints.

Key words: Au/Pd(P)/Cu, EPIG, Sn-Ag-Cu, Pd(P) thickness, CALPHAD, HSBS test

INTRODUCTION

Gold (Au) wire-bonding is a common packaging technology that is used for making interconnections between chips and chip-carrier boards. However, the price of Au has skyrocketed in recent years, which has prompted numerous attempts to find a satisfactory substitute for this noble metal in packaging applications. Copper (Cu) wire, possibly coated with a Pd or Au/Pd surface finish, has recently received a great deal of attention in the microelectronic industry due to its economic advantages and superior thermal and electrical properties as compared with Au wire.[1–3] The transition from a Au to Cu wire-bonding process has encouraged printed circuit board (PCB) and/or chip-carrier board manufacturers to seek an appropriate surface finish for the Cu metallization pads which promotes the bondability between the Cu wires and metallization pads. Direct deposition of electroless palladium/immersion gold (EPIG) bilayers over the Cu, i.e., Au/Pd(P)/Cu, is now being considered and adopted by the electronic industry. The Au/Pd(P) films are deposited with a thickness combination of (0.05 μm to 0.15 μm)/(0.1 μm to 0.2 μm). This material configuration, Au/Pd(P)/Cu, not only possesses compatibility with the Cu wire-bonding process but also significantly reduces the overall thickness of the surface finish from over 5 μm for the traditional Ni-bearing surface finish, e.g., Au/Ni or Au/Pd/Ni, to approximately 0.3 μm (i.e., EPIG). The reduction in surface finish thickness has promoted the development of fine-pitch interconnection technology with high-density input/output (I/O) terminals.

Data regarding the solderability of the EPIG surface finish are still seriously lacking in the literature. The objective of the current study is to evaluate the thermal reliability of EPIG in

(Received April 20, 2012; accepted July 9, 2012; published online August 1, 2012)

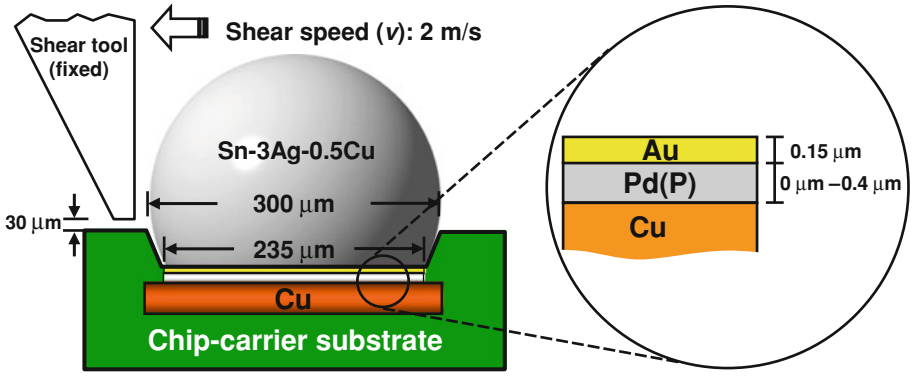

Fig. 1. Schematic illustrating the material sequence of the solder joint (before soldering) and the HSBS test setup in this study.

soldering applications, specifically focusing on the effect of Pd(P) thickness [$\delta_{Pd(P)}$] on the chemical interaction between the Sn-Ag-Cu alloy and Au/Pd(P)/Cu during soldering and subsequent solid-state aging. The effects of $\delta_{Pd(P)}$ on the reaction between Sn-3Ag-0.5Cu, i.e., 96.5Sn-3Ag-0.5Cu (wt.%), and a Au/Pd(P)/Ni(P) trilayer has recently been examined.[4–6] It was found that the Pd was immediately converted into $PdSn_4$ [or $(Pd,Ni)Sn_4$] after the removal of Au from the interface, and then spalled into the solder.[6,7] In turn, the underlying Ni(P) came into contact with the molten solder, forming the intermetallic compounds (IMCs) $(Cu,Ni)_6Sn_5$, Ni_2SnP, and Ni_3P. The growth of the former two phases, i.e., $(Cu,Ni)_6Sn_5$ and Ni_2SnP, strongly depended on $\delta_{Pd(P)}$.[4,5] As $\delta_{Pd(P)}$ increased, the morphology of the $(Cu,Ni)_6Sn_5$ changed from a layered structure to a discontinuous feature, and an undesirable, thick Ni_2SnP layer was formed. The dependence of the microstructures on $\delta_{Pd(P)}$ was attributed to the separation of P from the Pd(P) film during the early stage of the soldering reaction, which then nucleated as a dense Ni_2SnP layer over the Ni(P) substrate that dominated over the growth of the $(Cu,Ni)_6Sn_5$.[4,5] Additionally, the mechanical properties of solder joints have also been examined.[4–6] The shear strength obtained from the high-speed ball shear (HSBS) test strongly correlated with $\delta_{Pd(P)}$.[4,5] After one reflow, the shear strength of the solder joints increased as $\delta_{Pd(P)}$ increased; however, the opposite was observed when the joints underwent a multiple reflow process or solid-state aging treatment.[4,5] The results of these studies[4–6] indicate that $\delta_{Pd(P)}$ is a very important factor for solder joint reliability. More detailed descriptions of $\delta_{Pd(P)}$ effects can also be found in the literature.[4–6] Thus, observing the effect of $\delta_{Pd(P)}$ on solderability when Au/Pd(P) is directly deposited over the Cu pads is of great interest. In this study, the thickness of the Pd(P) layer was varied from 0 μm to 0.4 μm. The correlation between the interfacial microstructures and mechanical properties of the solder joints in response to various $\delta_{Pd(P)}$ values was established in this study.

EXPERIMENTAL PROCEDURES

Figure 1 illustrates the sequence of materials used for making the solder joint and the setup of the HSBS test utilized in this study. The metallization pad was composed of a trilayer Au/Pd(P)/Cu structure; the diameter of the opening in the Cu pad was 235 μm, the Au thickness (δ_{Au}) was 0.15 μm, and the Pd(P) thicknesses, i.e., $\delta_{Pd(P)}$, were 0 μm, 0.15 μm, 0.3 μm, and 0.4 μm. The thickness values were determined using a calibrated x-ray fluorescence (XRF) spectrometer (Seiko 9550), and were subsequently verified by cross-sectional analysis via focused ion beam (FIB). A specific amount of P (2% to 5%[7]) was codeposited with the Pd plating layer because a hypophosphite alkaline-based solution was employed in the plating process.

Before soldering, a fixed amount of rosin mildly activated (RMA) flux was smeared on the metallization pads, and solder balls with diameter of 300 μm were planted automatically using a solder ball placement system with a flux dispenser (Shinapex SSBM-03F). The solder balls consisted of 96.5 wt.% Sn, 3 wt.% Ag, and 0.5 wt.% Cu (hereafter termed Sn-3Ag-0.5Cu). The chip-carrier board (Fig. 1) was then subjected to an infrared (IR)-enhanced reflow oven. The peak reflow temperature was 260°C, and the reflow time, i.e., the time period above the melting point of the Sn-3Ag-0.5Cu alloy (~217°C), was 80 s. Following reflow, solder joints were subjected to isothermal aging at 180°C for a scheduled time period in the range of 0 h (as-reflow) to 1000 h.

After the aging treatment, solder joints were cross-sectioned and metallographically polished to reveal the interior microstructures. Field-emission scanning electron microscopy (FE-SEM) was employed to examine detailed microstructures of the reaction products. The composition of each phase was determined using electron probe microanalysis (EPMA; JEOL JXA-8200 and JXA-8500F).

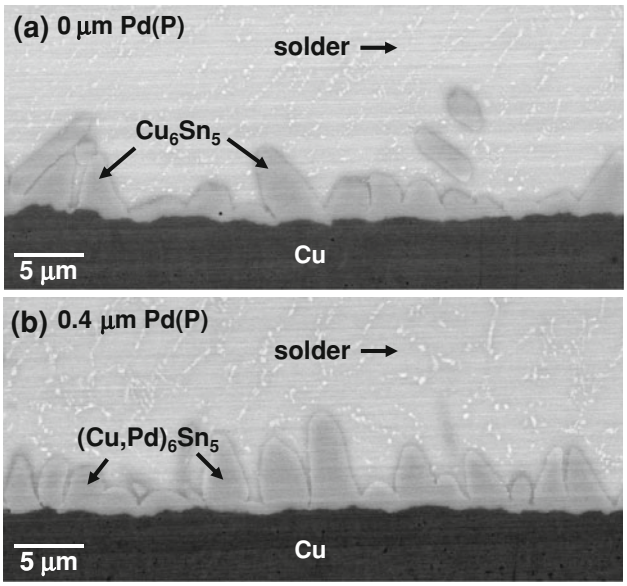

Fig. 2. Backscattered electron micrographs showing the interfacial microstructures between Sn-3Ag-0.5Cu and Au/Pd(P)/Cu after reflow. The thickness of Au is 0.15 μm and that of Pd(P) is 0 μm (a) and 0.4 μm (b).

At least three measurements were made for every data point, and the average value is reported. To evaluate the effect of $\delta_{Pd(P)}$ on the mechanical properties of the solder joints, a HSBS test with a shear speed of 2 m/s was performed using a bond tester (DAGE 4000HS) equipped with a 3-kg shear module and a 300-μm-wide shear tool (SHEAR-300HS-4). An illustration of the HSBS setup is shown in Fig. 1. The chip-carrier boards were adhered to glass slides (1 mm thick) using a cyanoacrylate glue to rigidly mount the substrates to the clamping fixture of the bond tester.[8] At least 15 measurements were determined for each data point, and average values with error bars are reported.

RESULTS

As-Reflow

The as-reflow microstructures of the Sn-3Ag-0.5Cu/Au/Pd(P)/Cu interface are shown in Fig. 2, where δ_{Au} is 0.15 μm and $\delta_{Pd(P)}$ is 0 μm (a) and 0.4 μm (b), respectively. The results for $\delta_{Pd(P)}$ = 0.15 μm and $\delta_{Pd(P)}$ = 0.3 μm were similar to those of $\delta_{Pd(P)}$ = 0 μm and 0.4 μm and are omitted for clarity. As can be clearly seen in Fig. 2, the Au/Pd(P) bilayers were eliminated from the solder/Cu interface, where a scallop-like IMC layer was formed immediately after reflow. This layer was identified by EPMA as Cu_6Sn_5 that might contain an additional amount of Pd (2.5 at.% to 3.8 at.%) in the Pd(P)-deposited cases. According to literature,[8,9] Pd atoms predominantly substitute for Cu in Cu_6Sn_5; thus, the compound layer formed in the present work is more properly referred to as $(Cu,Pd)_6Sn_5$. Based on EPMA, a significant amount of P was not detected in the reaction product, suggesting that the P constituent of the Pd(P) film did not participate in the chemical reaction between the molten solder and Cu. This scenario is unlike that occurred in the solder/Au/Pd(P)/Ni(P) system,[4,5] in which the P of the Pd(P) film might have been redeposited onto the substrate and crystallized with Ni and Sn into Ni_2SnP during the soldering reaction.

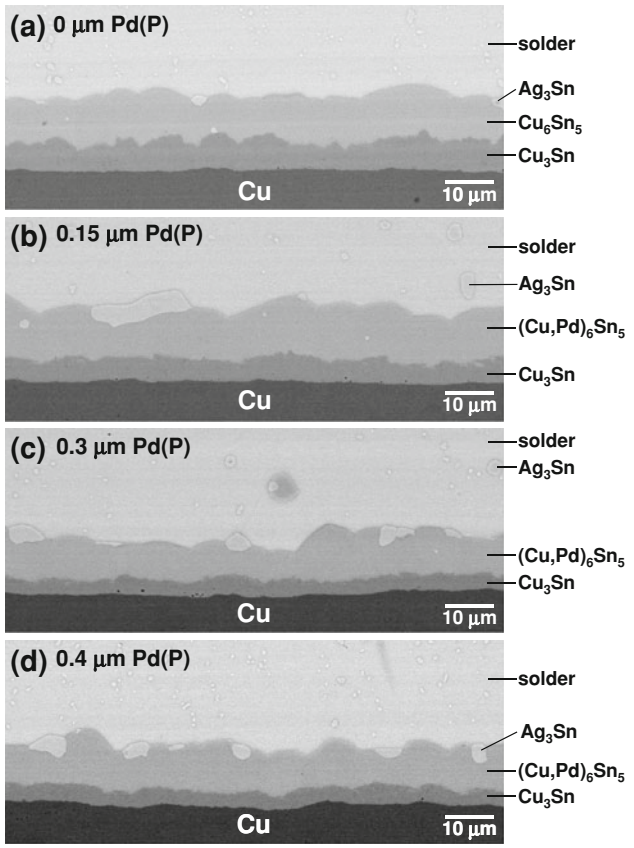

Fig. 3. Backscattered electron micrographs showing the interfacial microstructures between Sn-3Ag-0.5Cu and Au(0.15 μm)/Pd(P)/Cu after reflow and subsequent aging at 180°C for 1000 h. The thickness of Pd(P) is 0 μm (a), 0.15 μm (b), 0.3 μm (c), and 0.4 μm (d).

Solid-State Aging

Figure 3 shows cross sections of Sn-3Ag-0.5Cu/Au/Pd(P)/Cu solder joints after reflow and subsequent aging at 180°C for 1000 h, where $\delta_{Pd(P)}$ is 0 μm (a), 0.15 μm (b), 0.3 μm (c), and 0.4 μm (d). Several dramatic changes in the interfacial microstructures due to the aging treatment can be noted in this figure. First, significant growth of Cu_6Sn_5 [or $(Cu,Pd)_6Sn_5$] accompanies the morphological transition from scallop-type to layer-type. According to EPMA quantitative analyses, the Pd content in the Cu_6Sn_5 phase in fact increased with $\delta_{Pd(P)}$, being 1.1 at.% to 1.4 at.%, 1.6 at.% to 2.4 at.%, and 2.1 at.% to 3.4 at.% for $\delta_{Pd(P)}$ = 0.15 μm, 0.3 μm, and 0.4 μm, respectively. Second, an additional IMC layer appeared between the Cu_6Sn_5 and Cu (Fig. 3). With the aid of FE-EPMA, this layer was identified

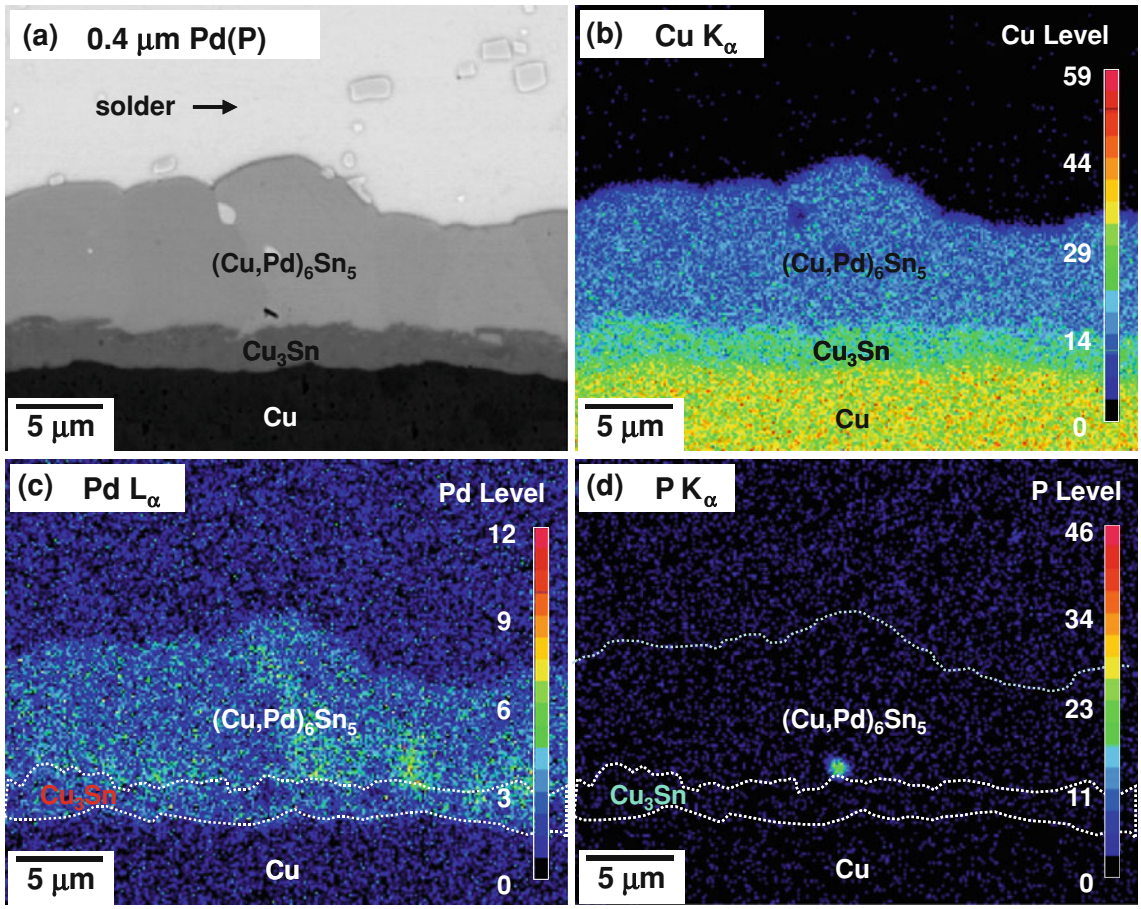

Fig. 4. (a) Backscattered electron micrograph of the interfacial microstructure between Sn-3Ag-0.5Cu and Au(0.15 μm)/Pd(P)(0.4 μm)/Cu after reflow and subsequent aging at 180°C for 500 h. FE-EPMA elemental mappings of Cu K_α (b), Pd L_α (c), and P K_α (d) x-rays corresponding to (a).

as Cu_3Sn. Pd incorporation into the Cu_3Sn phase was insignificant in all of the cases examined. The microstructural evolution of the Cu-Sn IMCs was consistent with findings reported in the literature.[10] It has been shown that generally only scallop-like Cu_6Sn_5 forms at the solder/Cu interface after reflow, whereas a dual-layer structure consisting of Cu_6Sn_5 and Cu_3Sn was established during subsequent solid-state aging.[10]

A backscattered electron micrograph of the interfacial microstructure between Sn-3Ag-0.5Cu and Au(0.15 μm)/Pd(P)(0.4 μm)/Cu after reflow and subsequent aging at 180°C for 500 h is shown in Fig. 4a. Figure 4b–d shows FE-EPMA x-ray mappings of Cu (b), Pd (c), and P (d) corresponding to the micrograph in Fig. 4a, which provides a visual depiction of the elemental distribution in the reaction zone. As can be clearly seen in Fig. 4, a specific amount of Pd was incorporated into the Cu_6Sn_5 phase, especially within the root of the compound layer. The high-Pd-content Cu_6Sn_5 might result from the soldering reaction, and this layer was gradually covered with low-Pd-content Cu_6Sn_5 in the subsequent solid-state aging. In contrast, less Pd was detected in Cu_3Sn (Fig. 4c), which is consistent with the results of the quantitative EPMA analysis. In addition, there was a small void of less than 0.5 μm diameter that existed between $(Cu,Pd)_6Sn_5$ and Cu_3Sn (Fig. 4a), which emitted strong P x-ray signals (Fig. 4d). The void was distinct from a typical Kirkendall void, which is usually spherical and aggregates near the root of the Cu_3Sn phase in the solder/Cu reaction system.[9,11–13] The domain of the P-containing void was too small to be resolved positively through FE-EPMA. Further examination using transmission electron microscopy is required to characterize such a small domain.

Based on analysis of Fig. 3, the growth thickness of Cu_6Sn_5 ($\delta_{Cu_6Sn_5}$) and Cu_3Sn (δ_{Cu_3Sn}) were both strongly correlated with $\delta_{Pd(P)}$ even though the entire thickness of the Cu-Sn IMCs ($\delta_{Cu_6Sn_5} + \delta_{Cu_3Sn}$) appeared to be insensitive to $\delta_{Pd(P)}$. To facilitate quantitative evaluation of the effect of $\delta_{Pd(P)}$ on the growth of the IMCs, $\delta_{Cu_6Sn_5}$ and δ_{Cu_3Sn} were measured individually and plotted against $\delta_{Pd(P)}$ in Fig. 5a and b, respectively. $\delta_{Cu_6Sn_5}$ increased proportionally with $\delta_{Pd(P)}$. The growth behavior of Cu_3Sn was approximately opposite to the upward trend observed in the $\delta_{Cu_6Sn_5}$-$\delta_{Pd(P)}$ plot (Fig. 5b).

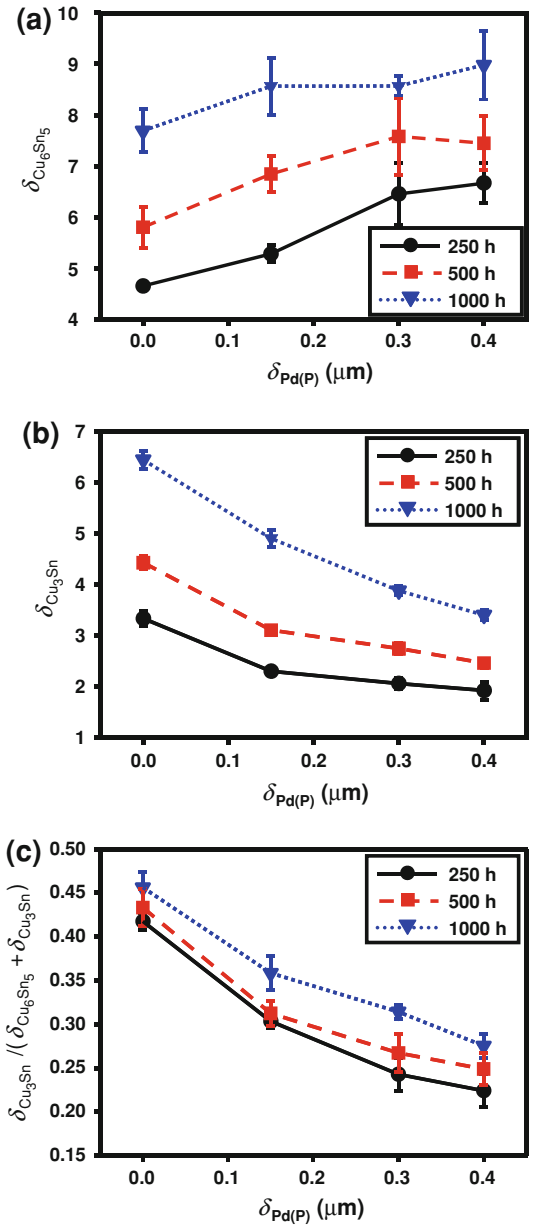

Fig. 5. $\delta_{Cu_6Sn_5}$ (a), δ_{Cu_3Sn} (b), and $\delta_{Cu_3Sn}/(\delta_{Cu_6Sn_5}+\delta_{Cu_3Sn})$ (c) as a function of $\delta_{Pd(P)}$ after aging at 180°C for 250 h (solid line), 500 h (dash line), and 1000 h (dotted line), respectively.

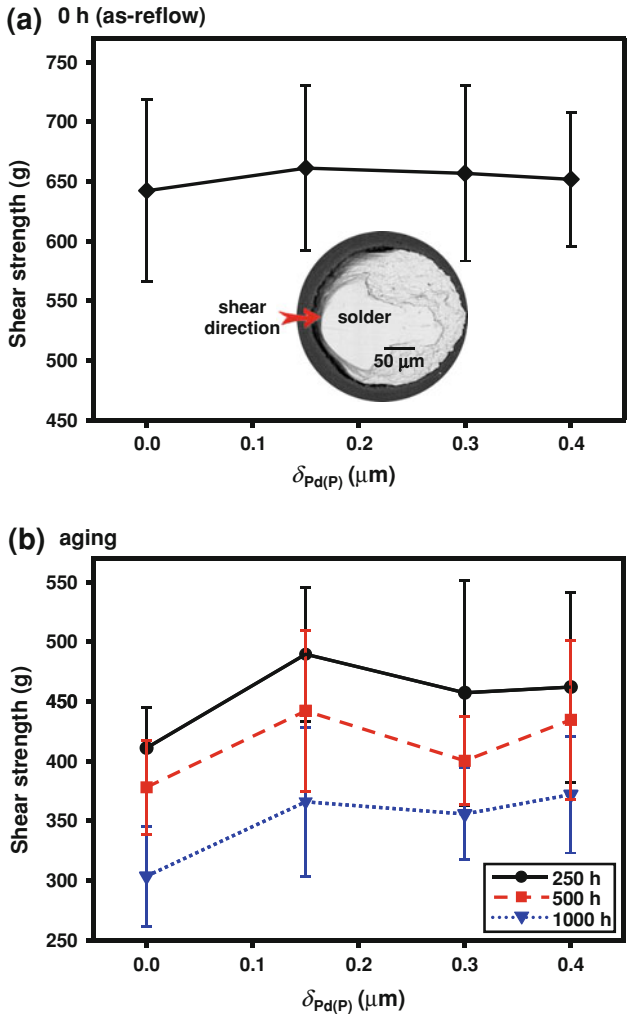

Fig. 6. Shear strength of Sn-3Ag-0.5Cu/Au/Pd(P)/Cu solder joints as a function of $\delta_{Pd(P)}$ after aging at 180°C for (a) 0 h (as-reflow), (b) 250 h (solid line), 500 h (dashed line), and 1000 h (dotted line). The inset in (a) displays the typical fracture surface (board side) of the as-reflow solder joint after HSBS testing.

Figure 5c depicts the $\delta_{Cu_3Sn}/(\delta_{Cu_6Sn_5}+\delta_{Cu_3Sn})$ ratio plotted against $\delta_{Pd(P)}$, which indicates that the thickness ratio increased inversely with $\delta_{Pd(P)}$ for all reaction times examined. For the $\delta_{Pd(P)}$ = 0 μm case, in which only a 0.15-μm-thick Au film was deposited over the Cu pads, the $\delta_{Cu_3Sn}/(\delta_{Cu_6Sn_5}+\delta_{Cu_3Sn})$ value gradually increased from 0.42 to 0.46, approximating the result observed for the Sn-Ag-Cu/Cu reaction system (0.45) in Ref. 10 in which no Au film was deposited. This corresponding result indicates that the Au plating (0.15 μm thick) played a minor role in the growth of Cu-Sn IMCs. Interestingly, the thickness ratio dramatically decreased from (0.4 to 0.45) to (0.25 to 0.3) as $\delta_{Pd(P)}$ increased (Fig. 5c). Figure 5 demonstrates that the growth of Cu_6Sn_5 was substantially enhanced while that of Cu_3Sn was suppressed as $\delta_{Pd(P)}$ increased.

HSBS Analysis

The mechanical response of the solder joints that resulted from using different $\delta_{Pd(P)}$ values was quantified with HSBS testing. Figure 6 shows a plot of joint strength as a function of $\delta_{Pd(P)}$ for various aging times: (a) 0 h (as-reflow), (b) 250 h (solid line), 500 h (dashed line), and 1000 h (dotted line). The strength values for the as-reflow case (Fig. 6a) did not exhibit a significant difference for $\delta_{Pd(P)}$ = 0 μm to 0.4 μm due to all of the fractures that predominantly occurred along the same region, i.e., the solder region, as shown in the inset of Fig. 6a. The joint strengths were degraded as a result of

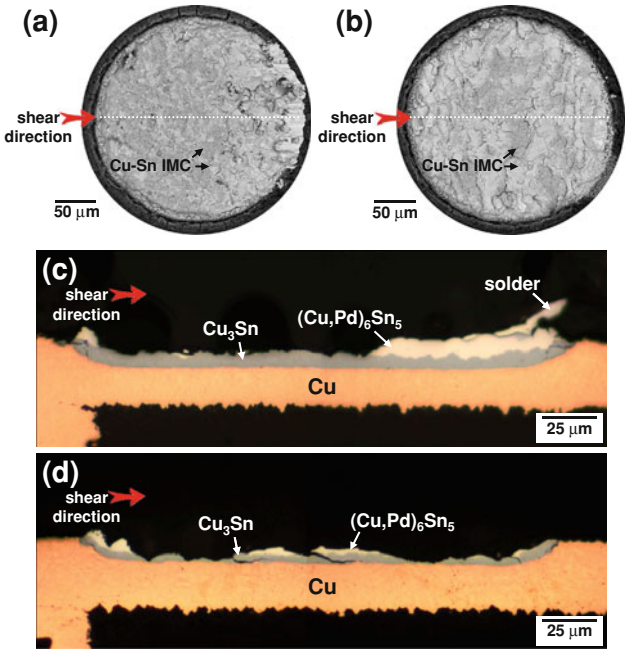

Fig. 7. (a, b) Electron micrographs showing the fracture surfaces of the Sn-3Ag-0.5Cu/Au/Pd(P)/Cu solder joints (board side) that had been aged at 180°C for 1000 h and then subjected to a HSBS test. (c, d) Cross-sectional view of the fracture surfaces shown in (a, b), respectively. The Au thickness is 0.15 μm and the Pd(P) thickness is 0 μm (a) and 0.4 μm (b), respectively.

subsequent aging (Fig. 6b); nevertheless, degradation was slightly improved with deposition of the Pd(P) film. These findings show that the mechanical properties of solder joints can be effectively modified with deposition of a Pd(P) film.

Typical fracture surfaces of Sn-3Ag-0.5Cu/Au/Pd(P)/Cu solder joints (board side) that were aged at 180°C for 1000 h and then underwent the HSBS test are shown in Fig. 7a, b. Figure 7c, d shows cross-sectional view of the fracture surfaces along the dotted lines depicted in Fig. 7a, b. In Fig. 7a, $\delta_{Pd(P)} = 0$ μm, and in 7b, $\delta_{Pd(P)} = 0.4$ μm. Figure 7 provides a better understanding of the effect of the Pd(P) film on the shear failure mode after the solid-state reaction. As shown in Fig. 7a, c, shear failure in the $\delta_{Pd(P)} = 0$ μm case occurred primarily via the initial propagation of a crack along the Cu_6Sn_5/Cu_3Sn interface and then along solder/Cu_6Sn_5 interface. In contrast, shear failure in the alternative case, i.e., $\delta_{Pd(P)} = 0.4$ μm, was translated into an interwoven fracture consisting of the Cu_6Sn_5/Cu_3Sn interface and the middle of the Cu_6Sn_5 layer (Fig. 7b, d), which possessed relatively high strength in comparison with the former case, i.e., $\delta_{Pd(P)} = 0$ μm. We argue that the modification of the $\delta_{Cu_3Sn}/(\delta_{Cu_6Sn_5} + \delta_{Cu_3Sn})$ value due to incorporation of Pd into Cu_6Sn_5 altered the failure mode, as shown in Fig. 7, which might produce various joint strengths.

DISCUSSION

The $\delta_{Pd(P)}$-dependent Cu-Sn IMC growth behavior, as shown in Fig. 5, invites further discussion. It is well accepted that the interdiffusion coefficient ($\tilde{D}_{int}$) plays a key role in the growth kinetics of a compound layer(s).[14] The growth of one compound layer can be retarded if its neighboring phase(s) possesses a relatively high $\tilde{D}_{int}$ value.[14] According to Ref. 15, the integrated interdiffusion coefficients of Cu_6Sn_5 ($\tilde{D}_{int}^{Cu_6Sn_5}$) and Cu_3Sn ($\tilde{D}_{int}^{Cu_3Sn}$) can be described as

$$\tilde{D}_{int}^{Cu_6Sn_5} = -(N_{Cu}^{Cu_6Sn_5} D_{Sn}^{*} + N_{Sn}^{Cu_6Sn_5} D_{Cu}^{*}) \frac{N_{Sn}^{Cu_6Sn_5} \Delta\mu_{Sn}}{RT}, \quad (1)$$

$$\tilde{D}_{int}^{Cu_3Sn} = -(N_{Cu}^{Cu_3Sn} D_{Sn}^{*} + N_{Sn}^{Cu_3Sn} D_{Cu}^{*}) \frac{N_{Cu}^{Cu_3Sn} \Delta\mu_{Cu}}{RT}, \quad (2)$$

where N_i^j is the mole fraction of element i in phase j; D_i^* is the tracer diffusivity of element i in each intermetallic phase; $\Delta\mu_i$ is the driving force for diffusion of element i through each intermetallic phase; R is the gas constant; and T is the temperature in Kelvin.

Quantitative EPMA measurements showed that $N_{Cu}^{Cu_6Sn_5}$, $N_{Sn}^{Cu_6Sn_5}$, $N_{Cu}^{Cu_3Sn}$, and $N_{Sn}^{Cu_3Sn}$ were essentially constants, regardless of $\delta_{Pd(P)}$. Taking the values of D_{Sn}^{*} and D_{Cu}^{*} as constants at given T, $\tilde{D}_{int}^{Cu_6Sn_5}$ and $\tilde{D}_{int}^{Cu_3Sn}$ increased proportionally with $\Delta\mu_{Sn}$ and $\Delta\mu_{Cu}$, respectively. In the present study, the values of $\Delta\mu_{Sn}$ and $\Delta\mu_{Cu}$ at 180°C, as well as the Gibbs free energies of face-centered cubic (fcc) Cu, Cu_3Sn (ε), and Cu_6Sn_5 (η) phases, were calculated through the computer coupling of phase diagrams and thermochemistry (CALPHAD) method, in which the Poly-3 module of the Thermocalc software was utilized. The calculation was based on descriptions of the Cu-Sn binary system,[16] and the outcome is schematically drawn in Fig. 8. Because Cu does not exhibit solubility in Sn, the β-Sn phase was treated as a pure element with free energy G^{β}.[16] The difference in the Gibbs free energies between *pure* Cu_6Sn_5 (G^{η}) and the same phase with a specific amount of dissolved Pd (2 at.%) (G^{η^*}) was calculated to be ~1852 J/mol (Fig. 8). The calculated free energies, shown in Fig. 8, were valid for the Cu-Sn binary system, and the G^{η^*} value was only the projection from the ternary phase onto the binary diagram surface. The decrease in the free energy after Pd incorporation was quite reasonable because a ternary compound usually has a lower Gibbs free energy than a binary one when they are isomorphous. The free energy of Cu_3Sn (G^{ε}) did not change substantially because only a very limited amount of Pd was dissolved into the phase and its stability would remain approximately the same as

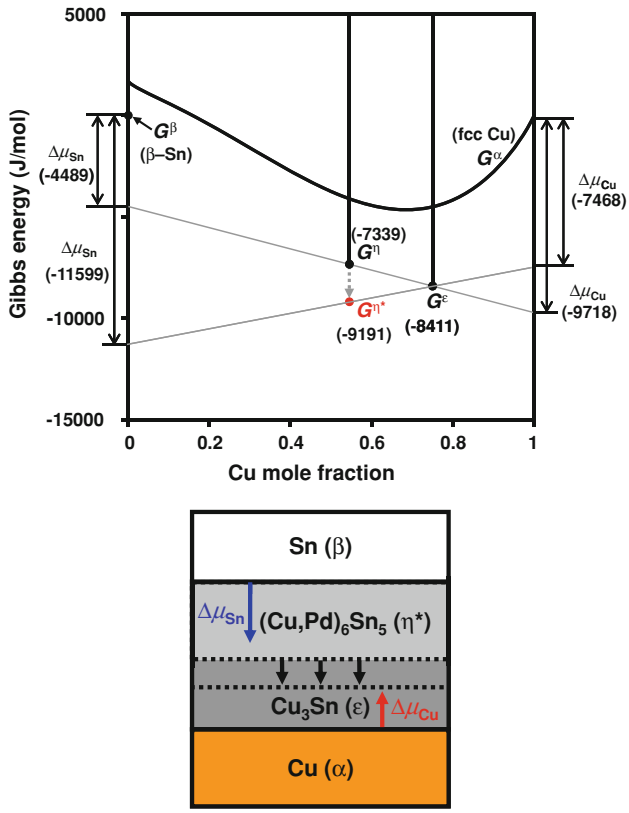

Fig. 8. Gibbs free energy diagram at 180°C showing the driving forces for atomic diffusion in the Cu/Sn couple.

pure Cu_3Sn. As observed in Fig. 8, at the same G^{ε} the decrease in the free energy ($G^{\eta} \rightarrow G^{\eta^*}$) enhanced the driving force for Sn diffusion [$\Delta\mu_{Sn}(-4489$ J/mol) $\rightarrow \Delta\mu_{Sn^*}$ ($-11{,}599$ J/mol)] but diminished that for Cu diffusion [$\Delta\mu_{Cu}(-9718$ J/mol) $\rightarrow \Delta\mu_{Cu^*_{Cu_6Sn_5}}$ (-7468 J/mol)]. This result increased $\tilde{D}_{int}^{Cu_6Sn_5}$ but decreased $\tilde{D}_{int}^{Cu_3Sn}$ (Eqs. 1–2), thereby enhancing $\delta_{Cu_6Sn_5}$ and suppressing δ_{Cu_3Sn} (Fig. 5). The calculated results provide a rationalization for why the growth of Cu_6Sn_5 was substantially enhanced and that of Cu_3Sn was suppressed as Pd(P) was deposited. Since the Pd content in the Cu_6Sn_5 increased as a function of $\delta_{Pd(P)}$, the $\delta_{Cu_3Sn}/(\delta_{Cu_6Sn_5} + \delta_{Cu_3Sn})$ ratio, as shown in Fig. 5c, decreased with increasing $\delta_{Pd(P)}$ was expected. Of course, the growth thickness of the IMCs (Cu_6Sn_5 and Cu_3Sn) depends not only on the diffusivity but also on the atomic concentration at the interface.[17] To determine the IMC thicknesses (i.e., δ_{Cu_3Sn} and $\delta_{Cu_6Sn_5}$), measurement of the atomic concentrations across the interfaces through energy-dispersive x-ray spectroscopy (EDX) or EPMA line scan is required in a subsequent study.

Another interesting finding that should be addressed is that no significant Kirkendall voiding occurred at the Cu_3Sn/Cu interface for all of the cases examined, even when the solder joints had been aged for 1000 h at 180°C (Fig. 3), and the resulting $\delta_{Cu_6Sn_5}$ and δ_{Cu_3Sn} were varied distinctly with $\delta_{Pd(P)}$. This result suggests that the formation of Kirkendall voids in the solder/Cu reaction system was independent of the growth of Cu_6Sn_5 and Cu_3Sn. This finding is inconsistent with that reported in Refs. 9,11–13 in which a series of Kirkendall voids aggregated at the Cu_3Sn/Cu interface or within the Cu_3Sn layer, especially when a large δ_{Cu_3Sn} was generated. The Kirkendall voiding induced by Cu_3Sn growth was attributed to a large difference in the diffusivity between Cu and Sn existing in the Cu_3Sn phase,[9,11–13] thereby causing a pronounced Kirkendall effect. However, according to recent research studies by Yu and Kim[18] and Yin et al.,[19,20] the growth of Cu_3Sn was not the exclusive cause of the Kirkendall voiding; the incorporation of organic impurities, e.g., bis-sodium sulfopropyl-disulfide, $C_6H_{12}O_6S_4Na_2$ (SPS),[18] or Cu^+-polyethylene glycol-Cl^-,[19,20] into the Cu substrate during electroplating was an equally important factor. Further analysis of the Cu substrate is required to confirm the viewpoint proposed in Refs. 18–20.

CONCLUSIONS

Interfacial reactions and the mechanical reliability between a Sn-3Ag-0.5Cu alloy and a Au/Pd(P)/Cu trilayer with constant Au thickness ($\delta_{Au} = 0.15$ μm) and various Pd(P) thicknesses ($\delta_{Pd(P)} = 0$ μm to 0.4 μm) were systematically investigated in this study. After a typical reflow, the Au/Pd(P) dual layer was completely eliminated from the interface, and scallop-like Cu_6Sn_5 [or $(Cu,Pd)_6Sn_5$] resulted between the solder and Cu. In the subsequent solid-state aging process (180°C), the reaction product, Cu_6Sn_5, tended to transition from scallop-type to layer-type morphology, and an additional IMC layer, Cu_3Sn, started to grow between Cu_6Sn_5 and Cu. The growth of Cu_6Sn_5 and Cu_3Sn were strongly dependent on $\delta_{Pd(P)}$. As $\delta_{Pd(P)}$ increased, the former phase (Cu_6Sn_5) was enhanced but the latter phase (Cu_3Sn) was suppressed. This finding was attributed to phase stabilization due to incorporation of Pd into the Cu_6Sn_5, causing an increase in $\tilde{D}_{int}^{Cu_6Sn_5}$ and a decrease in $\tilde{D}_{int}^{Cu_3Sn}$, thereby increasing the thickness of Cu_6Sn_5 but decreasing that of Cu_3Sn. The mechanical reliability of the solder joints after solid-state aging was also strongly $\delta_{Pd(P)}$ dependent. The HSBS test results showed that the shear failure mode was translated from the Cu_6Sn_5/Cu_3Sn interface ($\delta_{Pd(P)} = 0$ μm) to an interwoven fracture consisting of the Cu_6Sn_5/Cu_3Sn interface and the middle of the Cu_6Sn_5 layer ($\delta_{Pd(P)} = 0.4$ μm), resulting in an increase in the shear strength. The results of the aforementioned analyses indicate that Pd(P) deposition is beneficial to the thermal reliability of microelectronic solder joints.

ACKNOWLEDGEMENTS

This study was supported by the National Science Council (R.O.C.) through Grant Nos. NSC100-2221-E-155-018-MY3 and NSC101-2622-E-155-009-CC3. The authors would also like to acknowledge Nico Lee (Taiwan Uyemura Corp. Ltd.), Linda Huang

(Schmidt Scientific Taiwan Ltd.), Chung-Yuan Kao (National Taiwan University), and S.Y. Tsai (National Tsing Hua University) for their assistance with experiments.

REFERENCES

1. P. Ratchev, S. Stoukatch, and B. Swinnen, *Microelectron. Reliab.* 46, 1315 (2006).
2. Z.W. Zhong, *Microelectron. Int.* 26, 10 (2009).
3. B.K. Appelt, A. Tseng, Y.S. Lai, and C.H. Chen, *Proceeding of the 12th Electronics Packaging Technology Conference (EPTC)*, article number: 5702687, 479 (2010).
4. W.H. Wu, C.S. Lin, S.H. Huang, and C.E. Ho, *J. Electron. Mater.* 39, 2387 (2010).
5. C.E. Ho, W.H. Wu, L.H. Hsu, and C.S. Lin, *J. Electron. Mater.* 41, 11 (2012).
6. Y.M. Kim, J.Y. Park, and Y.H. Kim, *J. Electron. Mater.* 41, 763 (2012).
7. S.P. Peng, W.H. Wu, C.E. Ho, and Y.M. Huang, *J. Alloys Compd.* 493, 431 (2010).
8. C.E. Ho, L.H. Hsu, S.W. Lin, and M.A. Rahman, *J. Electron. Mater.* 41, 2 (2012).
9. T. Laurila, V. Vuorinen, and M. Paulasto-Kröckel, *Mater. Sci. Eng.* R68, 1 (2010).
10. T.Y. Lee, W.J. Choi, K.N. Tu, J.W. Jang, S.M. Kuo, J.K. Lin, D.R. Frear, K. Zeng, and J.K. Kivilahti, *J. Mater. Res.* 17, 291 (2002).
11. T. Laurila, V. Vuorinen, and J.K. Kivilahti, *Mater. Sci. Eng.* R49, 1 (2005).
12. K. Zeng, R. Stierman, T.C. Chiu, D. Edwards, K. Ano, and K.N. Tu, *J. Appl. Phys.* 97, 0245081 (2005).
13. C.P. Lin, C.M. Chen, C.H. Lin, and W.C. Su, *J. Alloys Compd.* 502, L17 (2010).
14. C.P. Chen and Y.A. Chang, *Diffusion in Ordered Alloys*, ed. B. Fultz, R.W. Cahn, and D. Gupta (Warrendale, PA: TMS, 1993), p. 169.
15. A. Paul, C. Ghosh, and W.J. Boettinger, *Metall. Mater. Trans.* A42, 952 (2011).
16. W. Gierlotka, S.W. Chen, and S.K. Lin, *J. Mater. Res.* 22, 3158 (2007).
17. K.N. Tu, J.W. Mayer, and L.C. Feldman, *Electronic Thin Film Science: For Electrical Engineering and Materials Scientist* (New York: Macmillan, 1992).
18. J. Yu and J.Y. Kim, *Acta Mater.* 56, 5514 (2008).
19. L. Yin and P. Borgesen, *J. Mater. Res.* 26, 455 (2011).
20. L. Yin, F. Wafula, N. Dimitrov, and P. Borgesen, *J. Electron. Mater.* 41, 302 (2012).